Bright and efficient sensitized near-infrared photoluminescence from an organic neodymium-containing composite material system.

Chen Lyu[1], Hongfei Li[1], Shufang Zhou[1], Guangfeng Liu[2], Peter B. Wyatt[3], William P. Gillin[1,4,*] and Huanqing Ye[4,1,*]

[1] Materials Research Institute and Department of Physics and Astronomy, Queen Mary University of London, Mile End Road, London E1 4NS, United Kingdom

[2] Laboratoire de chimie des polymères, Faculté des Sciences, Université Libre de Bruxelles (ULB), CP 206/01, Boulevard du Triomphe, 1050, Brussels, Belgium

[3] Materials Research Institute and Department of Chemistry, Queen Mary University of London, Mile End Road, London E1 4NS, United Kingdom

[4] Chromosol Ltd, The Walbrook Building, 25 Walbrook, London, EC4N 8A, United Kingdom

Supporting Information Placeholder

ABSTRACT: Intense organic neodymium (Nd^{3+}) emission is obtained with the near-infrared (NIR) emission equivalent in intensity to an organic semiconductor emitting material. The advantage of the Nd^{3+} emission is its narrow linewidth and NIR emission, which is enhanced by ~ 3000 times at low excitation power through an efficient sensitization effect from a composite organic sensitizer. This performance is optimized at high concentrations of Nd^{3+} ions and the organic perfluorinated system provides the ion excitations with a quantum efficiency of ~ 40%. The material system is applicable to thin films that are compatible with integrated optics applications.

Near-infrared (NIR) emitting material systems are advantageous to fabricate light sources for bioimaging devices, optical sensors and optical communications[1–6], as NIR wavelengths are less attenuated than visible light in these applications, fitting important optical wavelengths including the second bioimaging window and the o-band optical communications window. Given a suitable material candidate for these applications, high luminescence intensity is of vital importance and this performance will rely on the absorption/emission cross-sections (σ_{abs}/σ_{em}), radiative rates (R_{rad}), excited-state densities (N_{ex}), and quantum efficiencies (η). For example, semiconductor-like nanomaterials such as organic fluorescent compounds, quantum dots, perovskite, etc[7–12] can give intense visible emission (usually << 900 nm) with high quantum efficiencies due to their large radiative rates (R_{rad} = ~10^8 to 10^9 s^{-1}) and large cross-sections (σ_{abs}/σ_{em} = ~10^{-15} to 10^{-17} cm^2). Nevertheless, tuning the emission wavelength deeper into the NIR region usually fundamental changes their chemistry,[13,14] which detrimentally affects performance. NIR lanthanide materials such as neodymium-, ytterbium- and erbium-doped materials utilize the advantages of their intrinsic NIR emission at > 1 μm, therefore lanthanide doped nanoparticles or organic complexes have long been under development as alternatives.[15,16] However, the drawback is that the partially forbidden 4f-4f transitions of lanthanide ions result in weak emission/absorption cross-section (σ_{em} / σ_{abs} = ~10^{-21} to 10^{-20} cm^2) and a low radiative rate (R_{rad} = ~ 10^2 to 10^3 s^{-1}). These parameters are orders of magnitude smaller than in semiconductor materials and suggest very high excitation powers are inevitably required to produce strong luminescence. Also, high lanthanide ion concentrations induce a significant self-quenching effect[17,18] that tends to limit the intensity that can be achieved. Moreover, NIR lanthanide containing materials are easily quenched by hydrogen containing organic moieties such as C-H, O-H, N-H, etc.[19,20] This quenching effect is attributed to vibrational modes of those chemical bonds and can

greatly reduce the quantum efficiency of the NIR emission down to < 0.1%[20,21].

In this work, we report an exceptionally intense organic-semiconductor/neodymium (Nd^{3+}) material system emitting at 1.06 μm and 1.3 μm utilising a molecular composite of an organic neodymium (Nd^{3+}) molecule and one organic chromophore semiconductor molecule. The Nd^{3+} ion is coordinated within a cage of perfluorinated ligands to eliminate vibrational quenching so that its internal quantum efficiency (IQY) can reach ~40%, and the composite organic semiconductor chromophore gives an enormous sensitization effect to enhance the Nd^{3+} emission. The intense 1.06 μm emission fits the second bioimaging window; the 1.3 μm emission matches the optic-communication O-band, and the material system is easy to fabricate as thin films. These properties suggest a potential candidate of integrated light sources for those applications. The perfluorianted Nd^{3+} complex is Nd(F-TPIP)$_3$ where the Nd^{3+} ion is incorporated with three tetrakis(pentafluorophenyl)imidodiphosphinate (F-TPIP$^-$) ligands. Zn(F-BTZ)$_2$[22,23], a perfluorinated analog of Zn(BTZ)$_2$, which is an organic semiconductor material used for fabricating OLEDs, is the chromophore sensitizer component, where F-BTZ$^-$ refers to the conjugate base of 2-(tetrafluoro-2-hydroxphenyl)tetrafluorobenzothiazole. The enormous enhancement of Nd^{3+} emission by a factor of ~ 3000 is attributed to the energy transfer (ET) from the Zn(F-BTZ)$_2$ excitons to the Nd^{3+} ions. It is noteworthy that the luminescence intensity of Nd^{3+} at the NIR range is almost as high as the emission intensity of Zn(F-BTZ)$_2$ at the visible. That gives good evidence of intense NIR luminescence from Nd^{3+} doped material system with a low pump power and reasonably high Nd^{3+} concentration.
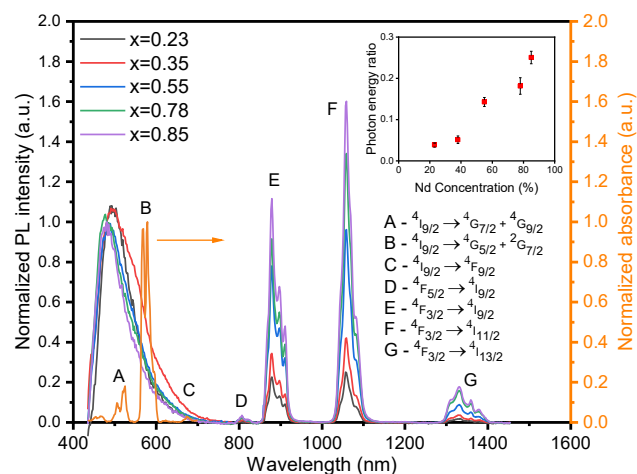
Result

A - $^4I_{9/2} \rightarrow {}^4G_{7/2} + {}^4G_{9/2}$
B - $^4I_{9/2} \rightarrow {}^4G_{5/2} + {}^2G_{7/2}$
C - $^4I_{9/2} \rightarrow {}^4F_{9/2}$
D - $^4F_{5/2} \rightarrow {}^4I_{9/2}$
E - $^4F_{3/2} \rightarrow {}^4I_{9/2}$
F - $^4F_{3/2} \rightarrow {}^4I_{11/2}$
G - $^4F_{3/2} \rightarrow {}^4I_{13/2}$

Figure 1. Absorption spectrum of Nd(F-TPIP)$_3$ and PL spectrum of [Nd(F-TPIP)$_3$]$_x$[Zn(F-BTZ)$_2$]$_{1-x}$ (x = 0.23, 0.38, 0.55, 0.78 and 0.85) thin films. The thickness of Zn(F-BTZ)$_2$ in these thin films is fixed to 50 nm. The excitation wavelength for PL spectra is 405 nm. All of the PL spectra are corrected for the responsivity of the utilized photon detectors and spectrometer gratings. The insert indicates the emission photon energy ratio between Nd^{3+} and Zn(F-BTZ)$_2$.

The Nd^{3+} absorption spectrum is obtained on an Nd(F-TPIP)$_3$ crystal that was grown by slow evaporation, shown as the orange curve in Figure 1 (to the left axis). This absorption spectrum demonstrates the characteristic Nd^{3+} transitions in the visible range and shows good overlap with the Zn(F-BTZ)$_2$ emission band. It is noteworthy that the absorption peak centred at 570 nm is a hypersensitive transition (^{4}I$_{9/2}$ → ^{4}G$_{5/2}$ + ^{4}G$_{7/2}$) and its transition strength is 5 to 10 times stronger than the others.

A series of composite thin films, [Nd(F-TPIP)$_3$]$_x$[Zn(F-BTZ)$_2$]$_{1-x}$ (x = 0.23, 0.38, 0.55, 0.78, 0.85) in which Zn(F-BTZ)$_2$ is employed at varied concentrations, were fabricated to characterise the sensitized

Nd^{3+} photoluminescence (PL). A 405 nm diode laser photoexcites these films to give the sensitized PL spectra in Figure 1 (to the left axis), corresponding to the intrinsic Nd^{3+} transitions as well as a broad emission band from 400 nm to 750 nm due to the Zn(F-BTZ)$_2$ emission. The Nd^{3+} PL intensity increases at higher Nd(F-TPIP)$_3$ concentrations and the Nd^{3+} 1060 nm peak emission becomes higher than that of the Zn(F-BTZ)$_2$ emission. Integrating all the Nd^{3+} emission bands and the Zn(F-BTZ)$_2$ band on an energy scale results in the ratios of the emitted energy of the Nd^{3+} compared to that from Zn(F-BTZ)$_2$, shown in the inset in Figure 1. As the Nd(F-TPIP)$_3$ concentration increases, the ratio rises from ~0.04 to ~0.27 and demonstrates that up to 27% of the total energy emitted is in the NIR region due to the Nd^{3+}. It is noteworthy that the Zn(F-BTZ)$_2$ emission cross-section is ~10^{-16} cm^2 with a nearly unity quantum efficiency for the fluorescence at room temperature (RT),[22] which is 3 orders of magnitude larger than the Nd^{3+} intrinsic absorption/emission cross-section of ~ 10^{-19} cm^2. Hence, the similar intensity implies the chromophore has generated a significant population of Nd^{3+} excited states.
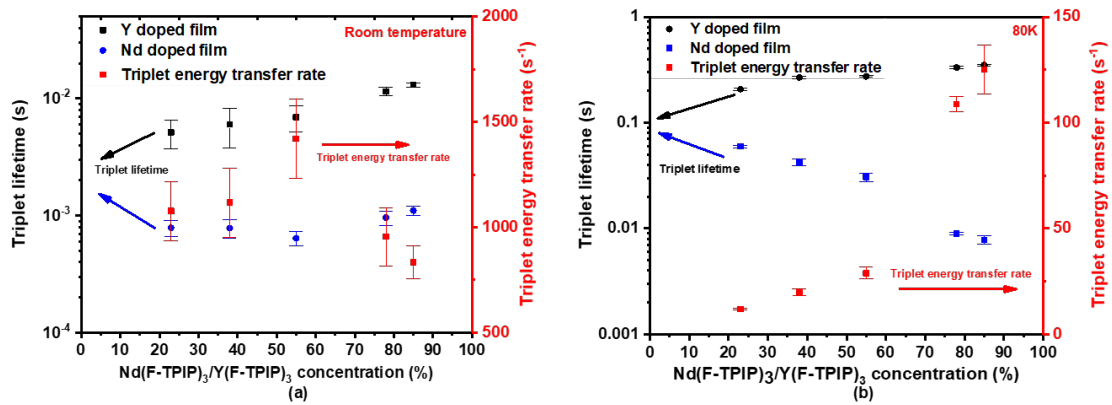

Figure 2. 550nm lifetime of [Nd(F-TPIP)$_3$]$_x$[Zn(F-BTZ)$_2$]$_{1-x}$ and [Y(F-TPIP)$_3$]$_x$[Zn(F-BTZ)$_2$]$_{1-x}$ thin films (x = 0.23, 0.38, 0.55, 0.78 and 0.85) at room temperature and 80K. Black dots indicate triplet lifetime in Y^{3+} doped film, blue dots represent triplet lifetime in Nd^{3+} doped films. The triplet energy transfer rate is given by red squares.

Time-resolved photoluminescence (TRPL) spectra of the composite films were recorded at 550 nm where the Zn(F-BTZ)$_2$ phosphorescence predominates due to the triplet emission[24]. A series of composite films of [Y(F-TPIP)$_3$]$_x$[Zn(F-BTZ)$_2$]$_{1-x}$ (x = 0.23, 0.38, 0.55, 0.78, 0.85) were used to compare the triplet emission properties by excluding the ET as Y^{3+} ions are optically inert. These decay traces are fitted with a three exponential decay function to give the lifetimes of triplet states, shown in the Table S1 to S4. In Figure 2 (a), the triplet lifetimes clearly become shorter in the presence of Nd(F-TPIP)$_3$ compared to the triplet lifetimes in the Y^{3+} doped films at room temperature. This indicates Nd^{3+} ions significantly quench triplet excitons due to the sensitization. The difference in the triplet lifetimes can be used to calculate the triplet ET rates (~800 to ~1300 s^{-1}) to Nd^{3+} excitations in Table S1 and S2. Also,

we calculate the Förster energy transfer rate (FRET) between Zn(F-BTZ)$_2$ and Nd^{3+} to give an estimated triplet ET rate varied from 728 ± 213 s^{-1} to 6186 ± 1814 s^{-1}, which are of the same order as the measured triplet ET rates, detailed in the SI. With the samples cooled to 80K, the thermally induced nonradiative quenching is reduced so that the triplet ET process to Nd^{3+} ions becomes more obvious where the triplet lifetimes can be quenched to ~ 7 ms from those that can be as long as ~ 330 ms in the Y(F-TPIP)$_3$ present samples. More evidently, a higher Nd(F-TPIP)$_3$ concentration makes the triplet lifetime much shorter and decreases from 40 ms to 7 ms. This suggests the triplet ET process is improved at a higher Nd^{3+} concentration, which might be expected as there are more Nd^{3+} ions to interact with each triplet.
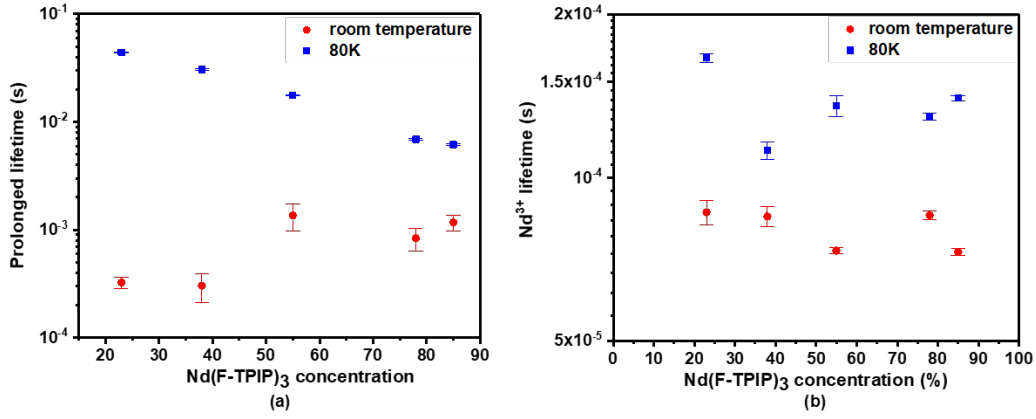
Figure 3. 1060 nm lifetime of $[Nd(F-TPIP)_3]_x[Zn(F-BTZ)_2]_{1-x}$ thin films (x = 0.23, 0.38, 0.55, 0.78 and 0.85) at room temperature and 80K. (a) Prolonged lifetime. (b) Nd^{3+} lifetime.

In Figure 3, the lifetime of Nd^{3+} 1060 nm is obtained to study of the influence on the Nd^{3+} depopulation process via the sensitization by $Zn(F-BTZ)_2$. At RT, they are around 80 μs, which correspond to a Nd^{3+} intrinsic decay process with an internal quantum efficiency (IQE) of ~ 24.7 ± 2.1 %, if we use an average literature reported value of 325 μs as the Nd^{3+} radiative lifetime[25,26]. There is another decay process with weak emission intensity but longer lifetime (blue dots), from 300 μs to 1.3 ms at different concentration films. Although the fitting of these long lifetimes has relatively large error bars, these prolonged lifetimes are probably longer than the radiative lifetime. However, these prolonged lifetimes cannot be seen in the TRPL spectrum of neat $Nd(F-TPIP)_3$ powder (Figure S2). These prolonged lifetimes have as comparable values as the triplet lifetimes in those $Nd(F-TPIP)_3$ present films according to Figure 2. Thus, we attribute them to the ET process from triplet as the long-lived triplet states, longer than the Nd^{3+} excited states, likely for them to re-excite some de-activated Nd^{3+} ions repeatedly. This process enables the replenishment of the excited state of Nd^{3+} ions until all the triplet states decay to the ground state. We believe this mechanism is consistent with those what have been presented and studied in a previous study of sensitized Yb^{3+} PL by $Zn(F-BTZ)_2$[27]. At 80K, the prolonged lifetimes are significantly extended as shown in Figure 3 (a) and (b). These prolonged lifetimes and their concentration dependence are again consistent with the measured triplet lifetimes in the $Nd(F-TPIP)_3$ composited films at 80K. Furthermore, the intrinsic lifetimes of Nd^{3+} 1060 nm PL are extended to ~ 125 μs, which improves the IQE of Nd^{3+} ions to 38.7 ± 5.3 % . That implies that low temperature restricts some thermally related non-radiative quenching routes to Nd^{3+} excited states.
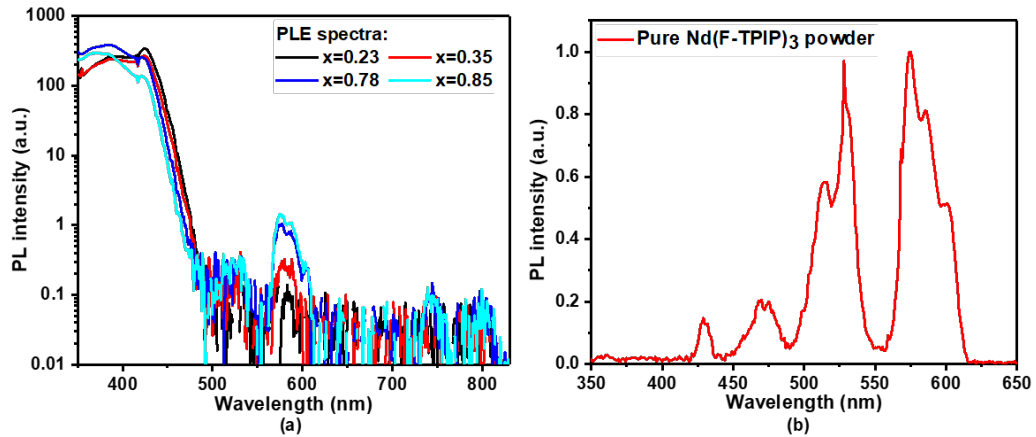

Figure 4. (a) PLE spectrum of $[Nd(F-TPIP)_3]_x[Zn(F-BTZ)_2]_{1-x}$ thin films (x = 0.23, 0.38, 0.78 and 0.85). (b) PLE spectrum of pure $Nd(F-TPIP)_3$ powder.

Figure 4a shows the photoluminescence excitation (PLE) spectra of different $Nd(F-TPIP)_3$ concentration present films at a wavelength of 1060 nm to visualize the sensitization from $Zn(F-BTZ)_2$. Those weak PLE peaks (at 520 nm, 570nm, 780 nm and 808 nm) are due to the intrinsic Nd^{3+} absorption. The PLE band from 350 nm to 450 nm corresponds to the absorption range of $Zn(F-BTZ)_2$ which is shown in Figure S1. The PLE spectrum (Figure 4b) of a pure $Nd(F-TPIP)_3$ powder shows only the direct excitation into the intrinsic Nd^{3+} transitions without a $F-TPIP^-$ contribution. Therefore, the ratio between the PL intensity generated by the absorption wavelength of $Zn(F-BTZ)_2$ and Nd^{3+} is a reliable measurement of the PL intensity enhancement via sensitization.

Figure S11 gives the PLE intensity enhancement with the $Nd(F-TPIP)_3$ concentration dependence. The enhancement factor is obtained from the PLE peak intensity ratio around 405 nm and 570 nm, which means excitation indirectly into $Zn(F-BTZ)_2$ and directly Nd^{3+} ions. The enhancement factor increases the sensitization from 400 for the 80% $Nd(F-TPIP)_3$ to >3000 for the 20% $Nd(F-TPIP)_3$. Rate equations are used to simulate the dynamics of the excited population of Nd^{3+} ions, elaborated in the SI. Equation S11 results in the simulated enhancement factor that is equivalent to the ratio of the sensitized Nd^{3+} population ($N_{Nd1\_sensitize}/N_{Nd1\_direct}$) and shows the simulated curve is consistent with our experimentally measured data with an estimated singlet ET rate of $8×10^8$ s^{-1}. In the modelling, the photon-emission rate of the excited Nd^{3+} ions (R_{Nd} × 24.7% IQE = ~ $2.8×10^3$ Hz) is about 5 orders of magnitude lower than that of the singlet emission (R_s =~ $5×10^8$ Hz). However, the sensitization effect increases the Nd^{3+} excitation densities ($N_{Nd1\_sensitize}$) by orders of magnitude to give a photon flux (~

$N_{Nd1\_sensitize} \times R_{Nd}$) comparable to that of the singlet emission ($\sim N_s \times R_s$), which results in the comparable emission intensities of the Zn(F-BTZ)$_3$ fluorescence and the Nd(F-TPIP)$_3$ emission displayed in Figure 1.

In conclusion, efficient sensitization from an organic sensitizer Zn(F-BTZ)$_2$ to Nd^{3+} ions enhance the excitation densities of Nd^{3+} ions by $\sim$ 3000 times maximumly at low excitation power. The enhancement results in comparable Nd^{3+} PL intensities to the fluorescence of the chromophore. The excited state dynamics are investigated by rate equation simulation to explain the concentration dependence of the phenomenon. Our results suggest a potential NIR emitting organic material system with high power efficiencies for luminescence at 1060nm and 1330 nm.

ASSOCIATED CONTENT

AUTHOR INFORMATION

Corresponding Author

Huanqing Ye - Chromosol Ltd, The Walbrook Building, 25 Walbrook, London, EC4N 8A, United Kingdom; Email: huaqing.ye@chromosol.com

William P. Gillin - Materials Research Institute and Dept of Physics and Astronomy, Queen Mary University of London, Mile End Road, London E1 4NS, United Kingdom; Email: w.gillin@qmul.ac.uk

NOTES
The authors declare no competing financial interests.

ACKNOWLEDGMENT

SUPPORTTING INFORMATION

Experimental details and supporting data, including Figure S1- S13 and Table S1 – S12.

REFERENCES

(1)   Katkova, M. A.; Pushkarev, A. P.; Balashova, T. V; Konev, A. N.; Fukin, G. K.; Ketkov, S. Y.; Bochkarev, M. N. Near-Infrared Electroluminescent Lanthanide [Pr (III), Nd (III), Ho (III), Er (III), Tm (III), and Yb (III)] N, O-Chelated Complexes for Organic Light-Emitting Devices. *J. Mater. Chem.* **2011**, *21* (41), 16611–16620.

(2)   Bünzli, J.-C. G. Lanthanide Light for Biology and Medical Diagnosis. *J. Lumin.* **2016**, *170*, 866–878.

(3)   Deiters, E.; Song, B.; Chauvin, A.; Vandevyver, C. D. B.; Gumy, F.; Bünzli, J. G. Luminescent Bimetallic Lanthanide Bioprobes for Cellular Imaging with Excitation in the Visible-light Range. *Chem. Eur. J.* **2009**, *15* (4), 885–900.

(4)   Yang, F.; Skripka, A.; Benayas, A.; Dong, X.; Hong, S. H.; Ren, F.; Oh, J. K.; Liu, X.; Vetrone, F.; Ma, D. An Integrated Multifunctional Nanoplatform for Deep-Tissue Dual-Mode Imaging. *Adv. Funct. Mater.* **2018**, *28* (11), 1706235.

(5)   Pedersen, J. E.; Brierley, M. High Saturation Output Power from a Neodymium-Doped Fluoride Fibre Amplifier Operating in the 1300 Nm Telecommunications Window. *Electron. Lett.* **1990**, *26* (12), 819–820.

(6)   Xu, J.-L.; Li, X.-L.; He, J.-L.; Hao, X.-P.; Yang, Y.; Wu, Y.-Z.; Liu, S.-D.; Zhang, B.-T. Efficient Graphene Q Switching and Mode Locking of 1.34 Mm Neodymium Lasers. *Opt. Lett.* **2012**, *37* (13), 2652–2654.

(7)   Wang, C.; Qiao, Q.; Chi, W.; Chen, J.; Liu, W.; Tan, D.; McKechnie, S.; Lyu, D.; Jiang, X.; Zhou, W. Quantitative Design of Bright Fluorophores and AIEgens by the Accurate Prediction of Twisted Intramolecular Charge Transfer (TICT). *Angew. Chemie* **2020**, *132* (25), 10246–10258.

(8)   Zhang, Y.; Hong, G.; Zhang, Y.; Chen, G.; Li, F.; Dai, H.; Wang, Q. Ag2S Quantum Dot: A Bright and Biocompatible Fluorescent Nanoprobe in the Second near-Infrared Window. *ACS Nano* **2012**, *6* (5), 3695–3702.

(9)   Li, X.; Zhao, Y.-B.; Fan, F.; Levina, L.; Liu, M.; Quintero-Bermudez, R.; Gong, X.; Quan, L. N.; Fan, J.; Yang, Z. Bright Colloidal Quantum Dot Light-Emitting Diodes Enabled by Efficient Chlorination. *Nat. Photonics* **2018**, *12* (3), 159–164.

(10)   Miao, Y.; Ke, Y.; Wang, N.; Zou, W.; Xu, M.; Cao, Y.; Sun, Y.; Yang, R.; Wang, Y.; Tong, Y. Stable and Bright Formamidinium-Based Perovskite Light-Emitting Diodes with High Energy Conversion Efficiency. *Nat. Commun.* **2019**, *10* (1), 1–7.

(11)   Tan, Z.-K.; Moghaddam, R. S.; Lai, M. L.; Docampo, P.; Higler, R.; Deschler, F.; Price, M.; Sadhanala, A.; Pazos, L. M.; Credgington, D. Bright Light-Emitting Diodes Based on Organometal Halide Perovskite. *Nat. Nanotechnol.* **2014**, *9* (9), 687–692.

(12)   Zhang, L.; Yang, X.; Jiang, Q.; Wang, P.; Yin, Z.; Zhang, X.; Tan, H.; Yang, Y. M.; Wei, M.; Sutherland, B. R. Ultra-Bright and Highly Efficient Inorganic Based Perovskite Light-Emitting Diodes. *Nat. Commun.* **2017**, *8* (1), 1–8.

(13)   Xie, C.; Zhao, X.; Ong, E. W. Y.; Tan, Z.-K. Transparent Near-Infrared Perovskite Light-Emitting Diodes. *Nat. Commun.* **2020**, *11* (1), 1–5.

(14)   Song, E.; Ding, S.; Wu, M.; Ye, S.; Xiao, F.; Zhou, S.; Zhang, Q. Anomalous NIR Luminescence in Mn2+-doped Fluoride Perovskite Nanocrystals. *Adv. Opt. Mater.* **2014**, *2* (7), 670–678.

(15)   Wang, T. T.; Ma, S. Y.; Cheng, L.; Luo, J.; Jiang, X. H.; Jin, W. X. Preparation of Yb-Doped SnO2 Hollow Nanofibers with an Enhanced Ethanol–Gas Sensing Performance by Electrospinning. *Sensors Actuators B Chem.* **2015**, *216*, 212–220.

(16)   Limpert, J.; Stutzki, F.; Jansen, F.; Otto, H.-J.; Eidam, T.; Jauregui, C.; Tünnermann, A. Yb-Doped Large-Pitch Fibres: Effective Single-Mode Operation Based on Higher-Order Mode Delocalisation. *Light Sci. Appl.* **2012**, *1* (4), e8–e8.

(17)   Bielawski, S.; Derozier, D.; Glorieux, P. Antiphase Dynamics and Polarization Effects in the Nd-Doped Fiber Laser. *Phys. Rev. A* **1992**, *46* (5), 2811.

(18)   Campbell, J. H.; Suratwala, T. I. Nd-Doped Phosphate Glasses for High-Energy/High-Peak-Power Lasers. *J. Non. Cryst. Solids* **2000**, *263*, 318–341.

(19)   Quochi, F.; Orru, R.; Cordella, F.; Mura, A.; Bongiovanni, G.; Artizzu, F.; Deplano, P.; Mercuri, M. L.; Pilia, L.; Serpe, A. Near Infrared Light Emission Quenching in Organolanthanide Complexes. *J. Appl. Phys.* **2006**, *99* (5), 53520.

(20)   Ye, H. Q.; Peng, Y.; Li, Z.; Wang, C. C.; Zheng, Y. X.; Motevalli, M.; Wyatt, P. B.; Gillin, W. P.; Hernández, I. Effect of Fluorination on the Radiative Properties of Er3+ Organic Complexes: An Opto-Structural Correlation Study. *J. Phys. Chem. C* **2013**, *117* (45), 23970–23975.

(21)   Ye, H. Q.; Li, Z.; Peng, Y.; Wang, C. C.; Li, T. Y.; Zheng, Y. X.; Sapelkin, a; Adamopoulos, G.; Hernández, I.; Wyatt, P. B.; Gillin, W. P. Organo-Erbium Systems for Optical Amplification at Telecommunications Wavelengths. *Nat. Mater.* **2014**, *13* (4), 382–386.

(22)   Li, Z.; Dellali, A.; Malik, J.; Motevalli, M.; Nix, R. M.; Olukoya, T.; Peng, Y.; Ye, H.; Gillin, W. P.; Hernández, I.; Wyatt, P. B. Luminescent Zinc(II) Complexes of Fluorinated Benzothiazol-2-Yl Substituted Phenoxide and Enolate Ligands. *Inorg. Chem.* **2013**, *52* (3), 1379–1387.

(23)   Glover, P. B.; Bassett, A. P.; Nockemann, P.; Kariuki, B. M.; Deun, R. Van; Pikramenou, Z. Fully Fluorinated Imidodiphosphinate Shells for Visible- and NIR-Emitting Lanthanides : Hitherto Unexpected Effects of Sensitizer Fluorination on Lanthanide Emission Properties. **2007**, 6308–6320.

(24)   Hu, J.; Wyatt, P. B.; Gillin, W. P.; Ye, H. Continuous Tuning of Organic Phosphorescence by Diluting Triplet Diffusion at the Molecular Level. *J. Phys. Chem. Lett.* **2018**, *9* (8), 2022–2024.

(25)   Krupke, W. F. Induced Emission Cross Sections in Neodymium Laser Glasses. *J. quantum electrinics* **1974**, *10(4)*, 450–457.

(26)   Werts, M. H. V; Jukes, R. T. F.; Verhoeven, J. W. The Emission Spectrum and the Radiative Lifetime of Eu 3+ in Luminescent Lanthanide Complexes. *Phys. Chem. Chem. Phys.* **2002**, *4* (9), 1542–1548.

(27)   Lyu, C.; Li, H.; Wyatt, P. B.; Gillin, W. P.; Ye, H. Prolonged and Efficient Near-Infrared Photoluminescence of a Sensitized Organic Ytterbium-Containing Molecular Composite. *J. Mater. Chem. C* **2020**, *8* (28), 9502–9505.

TOC Graphic